Functional screening in human cardiac organoids reveals a metabolic mechanism for cardiomyocyte cell cycle arrest

Richard J. Mills[a], Drew M. Titmarsh[a], Xaver Koenig[a,b], Benjamin L. Parker[c], James G. Ryall[d], Gregory A. Quaife-Ryan[a], Holly K. Voges[a], Mark P. Hodson[e,f,g], Charles Ferguson[h], Lauren Drowley[i], Alleyn T. Plowright[i], Elise J. Needham[c], Qing-Dong Wang[i], Paul Gregorevic[j], Mei Xin[k], Walter G. Thomas[a], Robert G. Parton[h,l], Lars K. Nielsen[e,f], Bradley S. Launikonis[a], David E. James[c], David A. Elliott[m,n], Enzo R. Porrello[a,d,m,1], and James E. Hudson[a,1]

[a]School of Biomedical Sciences, Faculty of Medicine, The University of Queensland, St. Lucia 4072, QLD, Australia; [b]Department for Neurophysiology and Pharmacology, Center for Physiology and Pharmacology, Medical University of Vienna, 1090 Vienna, Austria; [c]Charles Perkins Centre, School of Life and Environmental Science, The University of Sydney, Sydney 2006, NSW, Australia; [d]Department of Physiology, School of Biomedical Sciences, The University of Melbourne, Parkville 3010, VIC, Australia; [e]Metabolomics Australia Queensland Node, Australian Institute for Bioengineering and Nanotechnology, The University of Queensland, St. Lucia 4072, QLD, Australia; [f]Australian Institute for Bioengineering and Nanotechnology, The University of Queensland, St. Lucia 4072, QLD, Australia; [g]School of Pharmacy, The University of Queensland, St. Lucia 4072, QLD, Australia; [h]Institute for Molecular Bioscience, The University of Queensland, St. Lucia 4072, QLD, Australia; [i]Cardiovascular and Metabolic Diseases, Innovative Medicines and Early Development, AstraZeneca, Mölndal 431 83, Sweden; [j]Baker Heart and Diabetes Institute, Prahran 3004, VIC, Australia; [k]Department of Pediatrics, Division of Experimental Hematology and Cancer Biology, Cincinnati Children's Hospital Medical Center, Cincinnati, OH 45229; [l]Centre for Microscopy and Microanalysis, The University of Queensland, St. Lucia 4072, QLD, Australia; [m]Murdoch Childrens Research Institute, Royal Children's Hospital, Parkville 3052, VIC, Australia; and [n]School of Biosciences, The University of Melbourne, Parkville 3052, VIC, Australia

Edited by Eric N. Olson, University of Texas Southwestern Medical Center, Dallas, TX, and approved August 16, 2017 (received for review May 3, 2017)

The mammalian heart undergoes maturation during postnatal life to meet the increased functional requirements of an adult. However, the key drivers of this process remain poorly defined. We are currently unable to recapitulate postnatal maturation in human pluripotent stem cell-derived cardiomyocytes (hPSC-CMs), limiting their potential as a model system to discover regenerative therapeutics. Here, we provide a summary of our studies, where we developed a 96-well device for functional screening in human pluripotent stem cell-derived cardiac organoids (hCOs). Through interrogation of >10,000 organoids, we systematically optimize parameters, including extracellular matrix (ECM), metabolic substrate, and growth factor conditions, that enhance cardiac tissue viability, function, and maturation. Under optimized maturation conditions, functional and molecular characterization revealed that a switch to fatty acid metabolism was a central driver of cardiac maturation. Under these conditions, hPSC-CMs were refractory to mitogenic stimuli, and we found that key proliferation pathways including β-catenin and Yes-associated protein 1 (YAP1) were repressed. This proliferative barrier imposed by fatty acid metabolism in hCOs could be rescued by simultaneous activation of both β-catenin and YAP1 using genetic approaches or a small molecule activating both pathways. These studies highlight that human organoids coupled with higher-throughput screening platforms have the potential to rapidly expand our knowledge of human biology and potentially unlock therapeutic strategies.

heart development | regeneration | tissue engineering | pluripotent stem cells | metabolism

Maturation of cardiomyocytes occurs during early postnatal life and imposes numerous adaptations, including electrophysiological, structural, and metabolic changes (1), which occur coincident with loss of proliferative capacity and regenerative potential (2, 3). The discovery of key upstream drivers of cardiomyocyte maturation and cell cycle arrest remains one of the most important unanswered questions in cardiac biology. Discovery of these drivers would facilitate current attempts to promote cardiomyocyte maturation in vitro for drug discovery and to dedifferentiate adult cardiomyocytes in vivo for regenerative medicine.

There are considerable changes in metabolic substrate provision during early postnatal life. The mammalian heart relies on high concentrations of carbohydrates and the presence of insulin in utero but later switches to fatty acid-dominated substrates present in milk and low insulin levels postbirth (4). To adapt to these changes in substrates, cardiomyocytes up-regulate the genes required for fatty acid oxidation after birth (5). The importance of these metabolic adaptations for cardiomyocyte maturation has been difficult to study, because genetic disruption of fatty acid oxidation components in vivo can have a broad range of negative health impacts (6). Therefore, there is a need to develop alternative

Significance

Engineered cardiac muscle can be used to promote the structural and functional maturation of human pluripotent stem cell-derived cardiomyocytes (hPSC-CMs). However, previous studies have not yet produced cardiac tissues with metabolic and proliferative maturation. Here, we develop a 96-well screening platform and screen for cardiac maturation conditions in engineered cardiac muscle. We found that simulating the postnatal switch in metabolic substrates from carbohydrates to fatty acids promoted a switch in metabolism, DNA damage response, and cell cycle arrest in hPSC-CM. Our study shows that this mechanism can be harnessed to enhance the maturation of human hPSC-CM and cardiac tissues, which has major implications for stem cell sciences, drug discovery, and regenerative medicine.

Author contributions: R.J.M., D.M.T., X.K., B.L.P., E.R.P., and J.E.H. designed research; R.J.M., D.M.T., X.K., B.L.P., J.G.R., G.A.Q.-R., H.K.V., M.P.H., C.F., R.G.P., and J.E.H. performed research; R.J.M., D.M.T., X.K., B.L.P., J.G.R., G.A.Q.-R., H.K.V., M.P.H., C.F., L.D., A.T.P., Q.-D.W., P.G., M.X., W.G.T., R.G.P., L.K.N., B.S.L., D.E.J., D.A.E., E.R.P., and J.E.H. contributed new reagents/analytic tools; R.J.M., D.M.T., X.K., B.L.P., J.G.R., G.A.Q.-R., M.P.H., C.F., E.J.N., R.G.P., E.R.P., and J.E.H. analyzed data; and R.J.M., E.R.P., and J.E.H. wrote the paper.

Conflict of interest statement: R.J.M., D.M.T., E.R.P., and J.E.H. are listed as coinventors on a pending patent held by The University of Queensland that relates to the Heart-Dyno device and maturation medium, which are described in this paper. R.J.M., G.A.Q.-R., E.R.P., and J.E.H. are listed as coinventors on a pending patent held by The University of Queensland that relates to the reactivation of cardiomyocyte cell cycle for cardiac regeneration. L.D., A.T.P., and Q.-D.W. are employees of AstraZeneca.

This article is a PNAS Direct Submission.

Data deposition: The RNA-seq data reported in this paper have been deposited in the Gene Expression Omnibus (GEO) database, https://www.ncbi.nlm.nih.gov/geo (accession no. GSE93841), and the control medium vs. maturation medium human pluripotent stem cell-derived cardiac organoid proteomics data reported in this paper have been deposited in the PRIDE (accession no. PXD005736).

[1]To whom correspondence may be addressed. Email: enzo.porrello@mcri.edu.au or j.hudson@uq.edu.au.

This article contains supporting information online at www.pnas.org/lookup/suppl/doi:10.1073/pnas.1707316114/-/DCSupplemental.

approaches for studying the impact of cardiomyocyte metabolism on the maturation process.

Human pluripotent stem cells (hPSCs) are now widely used for the generation of defined human somatic cell types, including cardiomyocytes. Human pluripotent stem cell-derived cardiomyocytes (hPSC-CMs) have been used extensively for developmental studies, drug screening, disease modeling, and heart repair. However, lack of maturity and inappropriate responses to pharmacological agents have been identified as limitations in 2D or embryoid body-based differentiation strategies (7). In an effort to better simulate heart muscle structure and function, cardiac tissue engineering to form 3D engineered heart muscle has been used (8–14). These recent advances in human cardiac tissue engineering have greatly enhanced structural and functional maturation of hPSC-CMs. However, metabolic, transcriptional, and proliferative maturation have not yet been achieved.

We developed a 96-well device, the heart dynamometer (Heart-Dyno), for high-throughput functional screening of human pluripotent stem cell-derived cardiac organoids (hCOs) to facilitate screening for maturation conditions. The Heart-Dyno is designed to facilitate automated formation of dense muscle bundles from minimal cells and reagents, while also facilitating culture and automated force of contraction analysis without any tissue handling. Using the Heart-Dyno, we define serum-free 3D culture conditions that promote metabolic and proliferative maturation of hCOs. Furthermore, we uncover a metabolic mechanism governing hPSC-CM cell cycle arrest through repression of β-catenin- and Yes-associated protein 1 (YAP1)-dependent signaling.

Results

Heart-Dyno: A Miniaturized 96-Well hCO Screening Platform. To facilitate the automated formation and analysis of cardiac organoids comprising dense muscle bundles, we used SU-8 photolithography and polydimethylsiloxane (PDMS) casting to fabricate a 96-well plate containing culture inserts (Fig. 1*A*). We designed the elliptical geometry, such that a 3.5-μL volume containing 50,000 cardiac cells would automatically condense around two elastic posts over 2 d, forming hCOs 1 mm in length (Fig. 1*B* and Fig. S1*A*). hPSC-derived cardiac cells are composed of ∼70% α-actinin$^+$/CTNT$^+$ hPSC-CMs, with the rest being predominantly CD90$^+$ stromal cells (13). This ratio of hPSC-CMs to stromal cells is essential and optimal to form a functional hCO (13, 14). The elastic posts provide mechanical resistance to the contraction of the hCOs (Movie S1), which is required to enhance function (15). This design also allows contractile force to be approximated by tracking the movement of the poles (Fig. 1*C* and Movie S2), which we validated using force transducers (*SI Methods*). In addition, a custom-designed high-content imaging system was developed to capture 10-s videos of each hCO from each well at high speed (50 frames per 1 s). Video files were subsequently batch analyzed using a custom-written Matlab program to produce force traces and contraction data for each hCO (Fig. 1*D*). We further validated our 3D tissue culture and contraction analysis pipeline by assessing hCO responses to stimuli that alter the force of contraction (Fig. S1*B*) and prolong relaxation time (Fig. S1*C*). Importantly, the Heart-Dyno was able to predict physiological responses to known pharmacological agents, including compounds with human ether-a-go-go-related gene potassium channel (hERG) toxicity that entered the clinic and were subsequently withdrawn because of arrhythmogenic side effects (cisapride) (Fig. S1*C*).

In addition to semiautomated analyses of force of contraction, we also developed a protocol for postanalysis of hCOs for the expression of different markers using whole-mount immunostaining combined with high-content image analysis (Fig. 1*E*). We validated this approach using α-actinin and Ki-67 staining to detect the proproliferative effects of glycogen synthase kinase (GSK3) inhibition using CHIR99021 (16) (Fig. S1*D*). These initial studies validated the Heart-Dyno as a high-throughput, high-content screening platform that facilitates chronic stimulation as well as analysis of contractile properties and marker expression.

Screening for Optimal Metabolic Substrates for hCO Maturation. We next determined whether switching metabolism from glycolysis to fatty acid oxidation could induce hCO maturation. We screened a full factorial interplay between glucose and palmitate on cardiac maturation in serum-free medium. We chose to use palmitate as a fatty acid substrate, as it is one of the most abundant fatty acids circulating during the neonatal period, representing 36% of all long-chain free fatty acids (17). Cardiac maturation was assessed via three primary readouts: cardiac function (assessed by force of contraction), hPSC-CM proliferation as a marker of immaturity (assessed by Ki-67 expression), and expression of ventricular myosin light-chain 2 (MLC2v) as a maturation marker (18).

The hCO force of contraction showed a trend to increase with the addition of 10 and 100 μM palmitate under serum-free conditions (pooling all glucose concentrations for each palmitate concentration: $P = 0.007$ and $P = 0.07$ compared with 0 μM palmitate, respectively). The highest forces were produced within medium containing 1 mM glucose and 10 or 100 μM palmitate (Fig. 1*F*). Concurrently, MLC2v expression also increased with the addition of palmitate (Fig. 1*G*). All hCOs cultured in 100 μM palmitate in addition to hCOs cultured in 1 mM glucose with 10 μM palmitate had increased MLC2v expression relative to serum-free controls (5.5 mM glucose without palmitate). To assess if these serum-free conditions had any detrimental effects on cell viability, we performed ELISAs for lactate dehydrogenase and cardiac troponin I and found that their levels were unaffected by the addition of palmitate, indicating that our serum-free culture conditions in hCOs did not overtly cause cell death (Fig. S1 *E* and *F*). *SI Results* has more information regarding our iterative screening process, including optimization of serum-free medium and matrix composition.

Initial glucose-palmitate screening was performed in the presence of insulin, which is commonly used in most serum-free medium supplements to improve survival and function. However, as insulin induces glycolysis and could potentially promote proliferation through its actions on PI3K/GSK3 signaling (19), it could also be preventing cardiomyocyte maturation. We found that insulin was inducing hPSC-CM proliferation under serum-free conditions (1 mM glucose and 10 μM palmitate) (Fig. 1*H*). Although the removal of insulin reduced cell cycle activity, this condition could potentially have effects on cellular metabolism under serum-free conditions with 1 mM glucose and 10 μM palmitate. Therefore, we next screened the full factorial interplay between glucose and palmitate in the absence of insulin. We again saw an increase in force in the presence of palmitate, with significantly higher forces produced within tissues cultured in 100 μM palmitate, even in the presence of various concentrations of glucose (0.5, 1, and 5.5 mM glucose) (Fig. 1*I*). Palmitate once again promoted a trend to increased MLC2v expression (Fig. 1*J*). Culture of hCOs in serum-free medium (1 mM glucose with 100 μM palmitate and no insulin) also reduced cell cycle activity fourfold relative to the results obtained in control (CTRL) medium (Fig. 1*K*). These conditions allowed robust generation and culture of hCOs, derived from multiple hPSC lines, with viable, intact, and functional tissues produced greater than 90% of the time (Fig. 1*L*). We subsequently termed this medium "maturation medium" (MM) and performed extensive phenotypic analyses of hCOs using this maturation protocol (Fig. 1*M*).

MM Does Not Alter Cellular Composition in hCO. Consistent with the drop in Ki-67, we found that hCOs cultured in MM had a reduced number of cells compared with CTRL medium based on DNA intensity analysis (Fig. S2*A*). After dissociating hCOs, we determined that there are similar percentages of hPSC-CMs (α-actinin) present under both CTRL medium and MM conditions (Fig. S2 *B* and *C*). We also found a small but significant decrease in CD90$^+$ cells cultured in MM (13% CTRL to 10% MM,

$P < 0.05$) (Fig. S2*D*). Additionally, we used whole-mount immunostaining to examine multiple cardiac cell populations within the hCOs and found that hPSC-CMs (α-actinin or MLC2v), stromal cells (CD90), endothelial cells assembled into tubes (CD31), and epicardial cells (WT-1) were all present in tissues cultured in CTRL medium or MM (Fig. S2 *E* and *F*). In contrast to larger tissue formats, such as our recent publication (13), this suggests that endothelial structures are better supported in our dense miniaturized hCO format.

MM Does Not Further Enhance hPSC-CM Function in hCO. We analyzed the contractile properties of hCOs cultured in both CTRL medium and MM in detail. We found that hCOs cultured in MM had similar forces of contraction but reduced activation time [time from 50% activation to peak (Ta)] and reduced relaxation time [time from peak to 50% relaxation (Tr)] relative to hCO cultured in CTRL medium (Fig. 2*A*), reflecting the changes which occur during functional maturation during human cardiomyocyte development (20). To confirm these findings, we also profiled the contraction kinetics of hCOs derived from two additional cell lines: the human embryonic stem cell (hESC) line H9 and a commercially available human induced pluripotent stem cell (hiPSC) line. Both HES3-derived and hiPSC-derived hCOs displayed increased rates of contraction and reduced Ta in MM vs. CTRL medium. However, H9-derived hCO did not have increased rates of contraction or Ta in MM vs. CTRL medium (Fig. S3*A*). This indicates that changes in Ta are rate-dependent. In contrast, all lines tested had a reduced Tr in MM compared with those cultured in CTRL medium, regardless of rate (Fig. 2*A* and Fig. S3*A*). This may be caused by the reduction in endogenous ECM synthesis (Fig. 3 *F* and *G*), as ECM production also correlates with increased relaxation time in patients with heart disease (21).

We also assessed the chronotropic and inotropic responses to isoprenaline in hCOs cultured in both CTRL medium and MM. Isoprenaline increased the rate of contraction in both media (Fig. 2*B*). However, isoprenaline only induced an increase in the force of contraction in hCOs cultured in MM (Fig. 2*C*), which is indicative of a great contractile reserve under the culture conditions tested. We found that hCOs cultured in MM had a higher calcium EC_{50} for force of contraction (1.0 mM Ca^{2+}) than those cultured in CTRL medium (0.3 mM Ca^{2+}) (Fig. 2*D*). A low calcium EC_{50} may result in a blunted isoprenaline-induced inotropic response under our hCO culture conditions containing 1.8 mM Ca^{2+}, as the isoprenaline response depends on the contractile reserve (22). To investigate this, we assessed the effects of isoprenaline under highly controlled paced conditions (1 Hz) at the calcium EC_{50} for CTRL medium (0.3 mM) and MM (1.0 mM) hCO. Under these conditions, both CTRL medium and MM had similar increases in force of contraction and decreased 50% contraction time (Fig. 2*E*). The increased calcium EC_{50} in hCOs cultured in MM is indicative of maturation toward adult cardiac muscle [EC_{50} = 2.6–6.0 mM in adult (23)].

Calcium kinetics during contraction were also assessed using Fluo-4 AM calcium imaging on single cells dissociated from hCOs

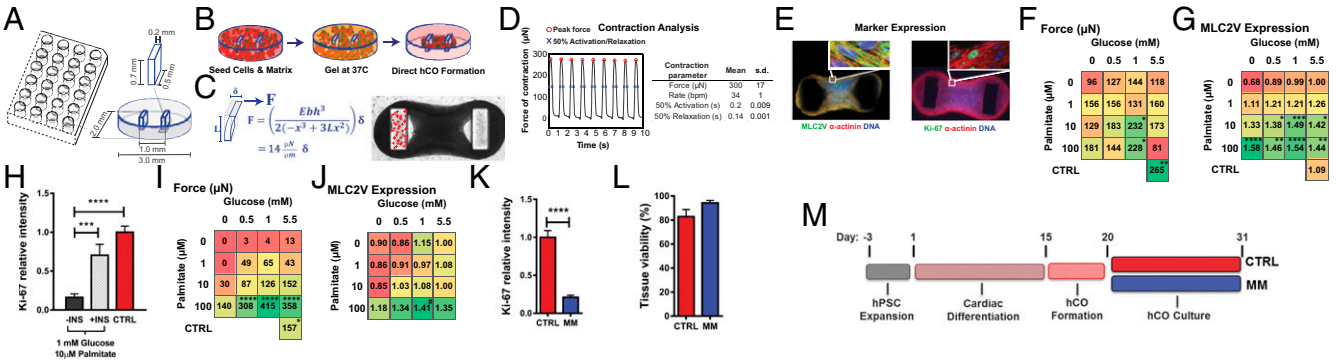

Fig. 1. The Heart-Dyno microtissue platform facilitates automated formation, mechanical loading, and analysis of hCOs. (*A*) Schematic representation of the 96-well plate Heart-Dyno. Each well has a culture insert containing an elliptical seeding well that contains two elastomeric posts. (*B*) Automatic tissue formation within the Heart-Dyno. hPSC-CMs and fibroblasts are seeded within ECM and allowed to gel for 30 min at 37 °C. Cells subsequently condense around the two elastomeric poles, resulting in the automated formation of an hCO. (*C*) Pole tracking can be used to approximate the force of contraction. (*Left*) Pole deflection schematic with force approximation formulas (*SI Methods*). Based on the parameters of our system, this results in a force equal to 14 μN/μm of postdeflection. (*Right*) Phase contrast image of a hCO; crosses on the left pole indicate tracking points selected by automated contraction analysis software. (*D*) Batch video analysis can be performed on each hCO to obtain contractile properties. (*Left*) Representative force trace curve. (*Right*) Overall contraction parameters ± SD from $n = 31$ hCO cultured for 7 d in CTRL medium. (*E*) Whole-mount immunostaining can be used to assess hCO marker expression for screening. Representative screening images with confocal close-up of MLC2v, Ki-67, and α-actinin immunostaining. (*F*) Screening identifies optimal glucose and palmitate concentrations for hCO force of contraction. Force heat map in response to a full factorial glucose (0, 0.5, 1, and 5.5 mM) and palmitate (0, 1, 10, and 100 μM) screen. Force was assessed after 5 d of serum-free culture after 2 d of hCO formation in CTRL medium; $n = 7$–13 from three experiments; HES3-derived hCOs (*SI Methods*). (*G*) Palmitate induces MLC2v expression. MLC2v heat map in response to a full factorial glucose (0, 0.5, 1, and 5.5 mM) and palmitate (0, 1, 10, and 100 μM) screen. MLC2v expression was assessed after 5 d of serum-free culture after 2 d of hCO formation in CTRL medium; $n = 7$–13 from three experiments; HES3-derived hCOs. MLC2v expression is relative to control serum-free conditions (5.5 mM glucose, no palmitate). (*H*) Ki-67 expression is induced by insulin. hCO were assessed after 11 d of serum-free culture after 5 d of hCO formation in CTRL medium; $n = 12$–13 from three experiments; HES3-derived hCOs. Ki-67 expression is relative to CTRL medium. (*I*) Screening identifies optimal glucose and palmitate levels in the absence of insulin. Force heat map in response to a full factorial glucose (0, 0.5, 1, and 5.5 mM) and palmitate (0, 1, 10, and 100 μM) screen without the presence of insulin. Force was assessed after 11 d of serum-free culture after 5 d of hCO formation in CTRL medium; $n = 6$–15 from three experiments; HES3-derived hCOs. (*J*) Palmitate induces MLC2v expression. MLC2v heat map in response to a full factorial glucose (0, 0.5, 1, and 5.5 mM) and palmitate (0, 1, 10, and 100 μM) screen in the absence of insulin. MLC2v expression was assessed after 11 d of serum-free culture after 5 d of hCO formation in CTRL medium; $n = 6$–9 from three experiments; HES3-derived hCOs. MLC2v expression is relative to control serum-free conditions (5.5 mM glucose, no palmitate). (*K*) Ki-67 expression is reduced in serum-free medium containing 1 mM glucose and 100 μM palmitate without insulin (now termed MM). hCOs were assessed after 11 d of serum-free culture after 5 d of hCO formation in CTRL medium. Ki-67 expression is relative to CTRL medium; $n = 6$–8 from two experiments; HES3-derived hCOs. (*L*) Culture of hCO maintains high tissue viability in CTRL medium or MM after 11 d of culture after 5 d of hCO formation in CTRL medium. Viability is defined as a live intact tissue with no deformities; $n = 16$ experiments with 733 and 717 tissues, respectively; HES3-derived hCOs. (*M*) Culture schematic of finalized cardiac maturation protocol indicating timing and duration of hPSC expansion, cardiac differentiation, and hCO formation and culture in CTRL medium or MM. Data are mean ± SEM; *SI Methods* has data variability for the heat maps (*F*, *G*, *I*, and *J*). #$P = 0.07$; *$P < 0.05$; **$P < 0.01$; ***$P < 0.001$; and ****$P < 0.0001$ using one-way ANOVA with Tukey's posttest (*H*), Dunnet's posttest relative to 5.5 mM glucose and no palmitate (*F*, *G*, *I*, and *J*), or *t* test (*K*).

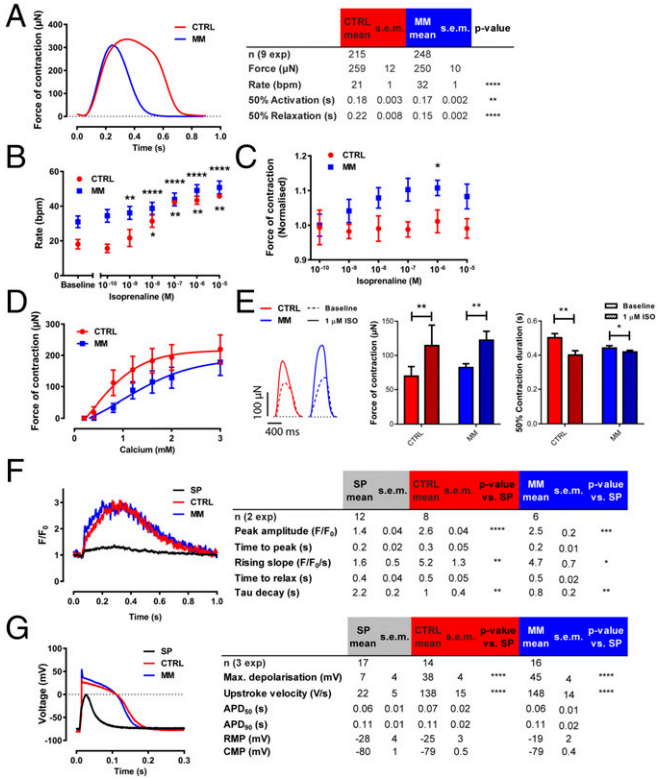

Fig. 2. Maturation of electrophysiological and contractile properties are determined by the tissue-engineered environment. (*A*) Representative individual contraction curves and contraction parameters of hCOs in CTRL medium or MM. (*B*) Isoprenaline stimulation induces an increased rate of contraction in hCOs; $n = 5$–7. (*C*) Isoprenaline increases the force of contraction in hCOs cultured in MM; $n = 5$–7 from two experiments. (*D*) hCOs cultured in MM have decreased calcium sensitivity. As isoprenaline stimulation experiments were performed in culture medium ($Ca^{2+} = 1.8$ mM), the effects of isoprenaline may be more pronounced at lower calcium concentrations; $n = 4$–7 from two experiments. (*E*) Isoprenaline increases force of contraction and decreases contraction duration under paced conditions (1 Hz) at the calcium EC_{50} (CTRL = 0.3 mM, MM = 1.0 mM); $n = 7$. (*F*) Representative individual calcium indicator (Fluo-4) recordings and parameters from individual hPSC-CMs dissociated from hCOs cultured in CTRL medium or MM paced at 1 Hz at 37 °C. (*G*) Representative individual action potential recordings and parameters from individual hPSC-CMs dissociated from hCOs cultured in CTRL medium or MM paced at 1 Hz at 37 °C. Data are mean ± SEM. The response curves to calcium of hCO in CTRL medium and MM are statistically significant using two-way ANOVA ($P < 0.05$) (*D*). APD, action potential duration; CMP, clamped membrane potential; RMP, resting membrane potential. $^*P < 0.05$; $^{**}P < 0.01$; $^{***}P < 0.001$; and $^{****}P < 0.0001$ using *t* test (*A* and *E*), two-way ANOVA (indicates difference relative to baseline; *B* and *C*), or ANOVA with Tukey's posttest (*F* and *G*).

at 1-Hz pacing (37 °C). Single-cell calcium recordings were obtained from the starting population (SP) of hPSC-CMs as a reference, and hPSC-CMs dissociated from hCOs in CTRL medium and MM (Fig. S3*B*). These experiments revealed that there was increased peak amplitude, rising slope, and decay in hCO relative to the SP, indicative of a more mature calcium handling system, but no differences were observed between hCOs cultured in the different media (Fig. 2*F*). The lack of difference in calcium handling kinetics between CTRL and MM hCOs (Fig. 2*F*) also supports the notion that the reduced contractile Tr in hCOs cultured in MM is caused by reduced ECM production rather than changes in hPSC-CM calcium handling properties.

We next determined the electrophysiological properties of hPSC-CMs using whole-cell patch-clamp recordings from single cells dissociated from hCOs cultured in CTRL medium or MM and SP hPSC-CMs as a reference. We found that the action potential profile in hPSC-CMs from hCOs in both CTRL medium and MM resembles that of adult ventricular cardiomyocytes (Fig. 2*G* and ventricular hPSC-CMs quantified in Fig. S3*C*). However, we found no differences between hPSC-CMs derived from CTRL medium or MM hCO (Fig. 3*G*). As the resting membrane potentials of the hPSC-CMs dissociated from hCOs were relatively depolarized (Fig. 2*G*), we also recorded electrophysiological parameters in situ in the hCOs using impaling electrodes (Fig. S3*D*). Using this approach, we found that the hPSC-CMs in situ had resting membrane potentials of approximately −60 mV (Fig. S3*D*). The depolarized membrane potentials in the initial patch-clamp experiments performed on enzymatically dissociated hPSC-CMs (Fig. 2*G*) were likely caused by the dissociation process. Importantly, the action potential recordings using impaling electrodes in situ also confirmed that hPSC-CMs in the hCOs in both CTRL medium and MM had adult-like ventricular action potentials (Fig. S2*D*). Together, these results suggest that the tissue-engineered culture environment is supportive of the development of in vivo-like functional maturation, as has been previously reported (10, 14).

MM Does Not Further Enhance Structural Organization Supported by hCO Culture. To determine whether there were other sarcomere-related changes in MM, we profiled the structural organization of the hPSC-CMs in the hCOs. Transmission electron microscopy (TEM) was used to confirm the presence of clear Z bands and I bands in the hCO in both CTRL medium and MM (Fig. S4*A*). This was confirmed using MLC2v and α-actinin staining revealing a highly organized expression pattern, with α-actinin localized to Z bands and MLC2v localized to I and A bands in hCOs cultured in either CTRL medium or MM (Fig. S4*B*). Titin and α-actinin staining also revealed clear delineation of α-actinin expression in the Z bands and titin expression in the I and A bands (Fig. S4*C*). The sarcomere length was ∼2.3 μm in both media (Fig. S4*D*), which is consistent with adult rather than immature cardiomyocytes (24). We also observed well-developed mitochondria (Fig. S4*E*) and t tubules (Fig. S4*F*) adjacent to the sarcomeres using TEM. We confirmed the presence of t tubules using caveolin-3 immunostaining (Fig. S4*G*).

Using TEM, we found that there were also highly organized intercalated discs (Fig. S4*H*), and we confirmed the formation of cell–cell junctions using pancadherin (Fig. S4*I*) and connexin 43 staining (Fig. S4*J*). Together, these results further suggest that the tissue-engineered culture environment is supportive of the development of in vivo-like structure, as has been previously reported (10, 14).

MM Induces Enhanced Maturation of Cardiac Developmental Factors, Metabolism, and Cell Cycle. To get a broader view of the effects of MM on hCOs, we next performed RNA sequencing (RNA-seq) on hCOs cultured in CTRL medium or MM and a commercially available adult heart sample (three pooled male hearts, 30–39 y old). Very few contaminating cell types from other lineages were present in the hCOs, with most markers for potentially contaminating lineages expressed at similar levels in hCOs and human adult heart tissue (Fig. S5*A*). When we examined markers of the most prominent cell types in the heart, we found that our protocol generated hPSC-CMs, epicardial cells, and fibroblastic cells, with a similar abundance of transcripts for these lineages present in hCO and human adult heart tissue (Fig. S5*B*). Endothelial transcripts were also present but at lower abundance, and leukocyte transcripts were low or absent in the hCOs relative to human adult heart tissue (Fig. S5*B*). These results are consistent with our flow cytometry and immunostaining (Fig. S2).

Principal component analysis (PCA) was performed to determine differences between our samples. For these analyses, we also included additional publically available reference data (GSE62913) including day 20 and 1-y-old hPSC-CMs, human fetal ventricles, and human adult hearts (25). When we used all transcripts (>10 counts per million), we found that hCOs clustered distinctly

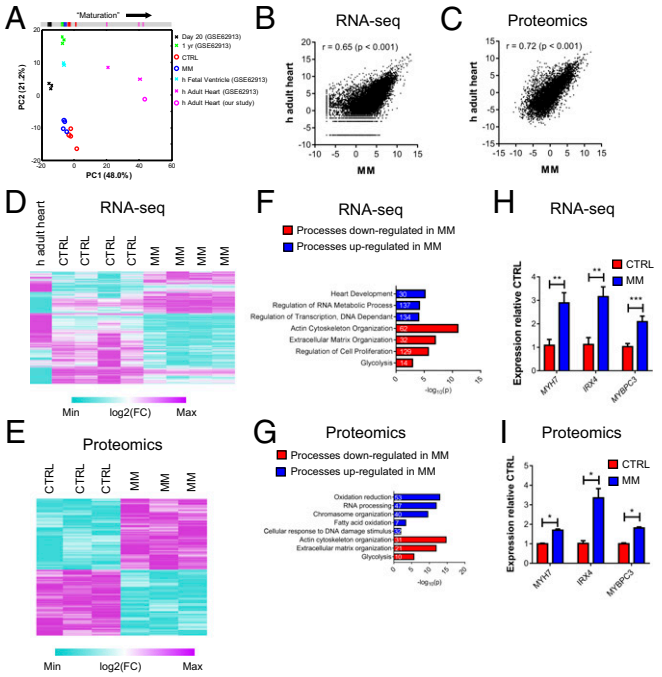

Fig. 3. Culture in MM induces transcriptional and proteomic maturation in hCOs. (*A*) PCA of RNA-seq data using a subset of genes identified by Delaughter et al. (27) to profile maturity (genes from table S6 in ref. 27). RNA-seq data derived from hCOs cultured in CTRL medium or MM ($n = 4$ experiments, each 20 pooled hCOs) and our human adult heart sample ($n = 1$, three pooled hearts) combined with RNA-seq data from Gene Expression Omnibus accession number GSE62913 (25) containing 2D hPSC-CMs at 20 d ($n = 3$) and 1 y ($n = 3$), human fetal ventricles ($n = 2$), and human adult hearts ($n = 2$). All genes were >10 counts per million for at least one sample. Bar at the top is a projection of PC1, the component that correlates with maturation. (*B*) Pearson correlation coefficient indicates that hCOs cultured in MM are significantly correlated to human adult heart tissue. Graph is of $\log_2$(cpm) of human adult heart ($n = 1$, three pooled hearts) or average gene expression of hCOs cultured in MM ($n = 4$). (*C*) Pearson correlation coefficient indicates that hCOs cultured in MM are significantly correlated to human adult heart tissue. Graph is of $\log_2$(iBAQ) of human adult heart ($n = 1$) or pooled hCOs cultured in MM ($n = 3$, each nine pooled hCO). iBAQ, intensity-based absolute quantification. (*D*) Clustered heat map of genes regulated (FDR < 0.05) between hCOs cultured in CTRL medium vs. MM. (*E*) Clustered heat map of proteins regulated (q value < 0.05) between hCOs cultured in CTRL vs. MM. (*F*) GO term analysis of RNA-seq reveals that multiple processes are decreased or increased in hCOs cultured in MM vs. CTRL medium. These are consistent with processes that occur during postnatal heart maturation (5). Numbers in the bars indicate numbers of genes identified in that particular process. (*G*) GO term analysis of proteomics reveals that multiple processes are decreased and increased in hCOs cultured in MM vs. CTRL medium. These are consistent with processes that occur during postnatal heart maturation (5). Numbers in the bars indicate numbers of genes identified in that particular process. (*H*) RNA-seq markers of maturation: genes in the cardiac development GO term, which are also up-regulated in proteomics data. (*I*) Proteomics markers of maturation: genes in the cardiac development GO term. Data are mean ± SEM. *$P < 0.05$; **$P < 0.01$; and ***$P <$ 0.001, FDR (*H*) or q value (*I*) for statistical analysis (*SI Methods*).

from other samples, indicating good reproducibility between experiments (Fig. S5*C*). However, no two conditions clustered together, which was most likely because of the influence of different cell populations being present in each different sample [i.e., hPSC-CM samples from Kuppusamy et al. (25) are pure, while our hCO samples and the heart tissues contain multiple cell types]. Indeed, hCOs have fewer endothelial cells and lack leukocytes (Fig. S5*B*), which are abundant in native heart tissue (26). In support of this notion, the top 25 Gene Ontology (GO) terms for the top 1,000 genes that were more highly expressed in human adult heart tissue relative to hCOs cultured in MM were mostly related to immune processes (Fig. S5*D*). Nevertheless, we used a similar approach as Delaughter et al. (27) to profile the developmental stage of our hCO by performing PCA on transcripts expressed in cardiomyocytes (table S6 in ref. 27) (795 transcripts >10 counts per million). We found that the hCOs from both CTRL medium and MM conditions in 1-y-old hPSC-CMs and human fetal ventricles clustered on principal component 1 (PC1) using this approach and were more mature than 20-d-old hPSC-CMs (Fig. 3*A*), consistent with the maturation profiling presented in the work by Delaughter et al. (27). Despite these differences, which are accentuated by PCA, we found that hCOs cultured in MM highly correlated to adult human heart tissue based on RNA-seq data (Fig. 3*B*). We also performed proteomics on hCOs cultured in CTRL medium or MM and adult human heart tissue and found that hCOs cultured in MM also closely resembled human adult heart tissue based on proteomic data (Fig. 3*C*).

We identified 3,856 transcripts and 855 proteins that were differentially regulated between hCOs in CTRL medium or MM [false discovery rate (FDR) < 0.05 and q value < 0.05, respectively] (Fig. S5 *E* and *F*). Using the differentially expressed genes (Fig. 3*D*) or proteins (Fig. 3*E*), we performed GO term analysis independently on the RNA-seq (Fig. 3*F*) and proteomic datasets (Fig. 3*G*). In both cases, reductions in glycolysis, ECM organization, and actin cytoskeleton organization were identified in hCO cultured in MM (Fig. 3 *F* and *G*). Processes that were consistently enhanced between the two datasets included RNA processing/regulation of RNA metabolic process and regulation of transcription/chromosome organization (Fig. 3 *F* and *G*). Interestingly, oxidation reduction, fatty acid oxidation, and cellular response to DNA damage stimulus were only up-regulated in the proteomic dataset (Fig. 3 *F* and *G*). These biological processes are highly indicative of mammalian postnatal maturation of cardiomyocytes in vivo (5, 28, 29), which additionally highlights the importance of performing proteomic analyses in addition to transcriptomics. Consistent with postnatal maturation, the GO term cell cycle regulation was reduced by MM specifically in the RNA-seq dataset, likely because of the low abundance of proteins involved in the cell cycle, even in CTRL medium (Fig. 3 *F* and *G*). The GO term heart development was also up-regulated in hCOs cultured in MM in the RNA-seq dataset (Fig. 3*F*), and key factors involved in cardiac maturation in this GO term (*MYH7*, *IRX4*, and *MYBPC3*) were also up-regulated in the proteomics analysis (Fig. 3 *H* and *I*). MYH7 is known to increase during human heart maturation (30), IRX4 nuclear translocation increases during postnatal cardiac maturation (31) and is critical for maintaining cardiac function (32), and cardiomyocytes undergo an additional round of division before postnatal cell cycle arrest in MYBPC3 KO mice (33). We also validated that sarcomeric isoforms known to switch/increase during maturation (24), such as *TTN N2B*, *MYH7/6*, and *TNNI3/1*, increased in hCO cultured in MM using quantitative PCR (qPCR) (Fig. S5*G*). Collectively, these results show that hCOs cultured in MM undergo multiple postnatal maturation processes, including induction of cardiac developmental factors, metabolic switching, DNA damage, and a reduction in cell cycle activity. However, our findings also highlight that hCO culture in MM specifically matures these processes, while other structural and functional properties associated with maturation are not further enhanced by culture in MM (as found in Fig. 2 and Figs. S3 and S4).

MM Induces a Metabolic Switch from Glycolysis to Fatty Acid Oxidation. Our RNA-seq and proteomics analyses (Fig. 3) revealed that hCO culture in MM represses many glycolysis components and activates many fatty acid oxidation components in hCO (Fig. S6). We next profiled metabolism of hCOs using the Seahorse XF Bioanalyzer mitochondrial stress test with an additional step to measure endogenous fatty acid oxidation using etomoxir (Fig. 4*A*). In support of a switch to fatty acid oxidation, hCOs from MM had a

higher maximal oxygen consumption rate (OCR) (Fig. 4*B*), OCR reserve (Fig. 4*C*), and increased fatty acid oxidation (Fig. 4*D*) under the Seahorse test conditions. These changes in oxidative capacity were associated with an increase in mitochondrial content (mtDNA) (Fig. 4*E*). As ATP uncoupling using carbonyl cyanide-4 (trifluoromethoxy) phenylhydrazone (FCCP) can lead to large increases in extracellular acidification rate in mature cardiomyocytes, even in the absence of glucose (34), we chose to use metabolomics to further profile glycolytic and branching pathway metabolic flux in hCO under CTRL medium and MM conditions. Metabolites in the glycolysis pathway as well as pathways branching from it, including hexosamine, pentose phosphate, and glycogen pathways, were all reduced in MM compared with CTRL medium (Fig. 4*F*). Together, our RNA-seq, proteomics, Seahorse data, and metabolomics confirm a switch in metabolism from glycolysis to fatty acid oxidation.

MM Inhibits Cell Cycle and Is Associated with Repression of β-Catenin and Induction of the DNA Damage Response. We firstly confirmed that MM induces a decrease in Ki-67 intensity in multiple additional hPSC cell lines (H9 and hiPSC) (Fig. S7 *A* and *B*). Additionally, we confirmed our initial whole-mount fluorescence intensity screening data (Fig. 1*K*) using high-resolution confocal microscopy staining and quantification of hPSC-CM cell cycle activity. We found that hCO culture in MM caused a reduction in percentage of hPSC-CMs in the cell cycle using the general cell cycle marker, Ki-67 (Fig. 5*A*), and the mitosis-specific marker, phosphohistone H3 (Ser10) (pH3) (Fig. 5*B*). hPSC-CM proliferation was markedly reduced in hCOs cultured in MM, with very low overall rates of hPSC-CM mitosis (~0.2% $pH3^+$ hPSC-CMs), which is similar to the postnatal human heart (35).

We next wanted to assess how metabolic substrates influenced the cardiac cell cycle. We performed a factorial experiment with glucose, insulin, and palmitate after the hCO formation phase. Importantly, all conditions had a similar force of contraction during the first 48 h of culture (Fig. S7*C*), indicating that the hCOs have similar functional properties and viability at this early stage, even in the absence of glucose and palmitate (in contrast to longer term cultures) (Fig. 1*I*). In these studies, we specifically examined the Wnt/β-catenin signaling pathway, as we have previously identified CHIR99021 as one of the most potent activators of human cardiomyocyte proliferation (16) and have also found this pathway to be transcriptionally repressed during postnatal maturation (5). As a readout of β-catenin activity in our screen, we performed quantification of activated β-catenin using an antibody that only binds to activated, nuclear-localized β-catenin (36). Activated β-catenin was highly dependent on insulin, regardless of the presence of either glucose or palmitate (Fig. 5 *C* and *D*), as was proliferation (Fig. 5*E*), and there was a highly significant correlation between activated β-catenin and Ki-67 intensity (Fig. 5*F*) (over all hCOs in all conditions). Despite this dependence on insulin signaling for proliferation 2 d after culture in MM, the addition of insulin after 11 d in MM was not sufficient to reactivate hPSC-CM proliferation (Fig. 5 *G*–*I*). This indicates that longer term culture in MM induces desensitization of hPSC-CMs to the proliferative actions of insulin.

As mature cardiomyocytes are largely refractory to proliferative stimuli, we next wanted to test whether potent cardiomyocyte mitogens could stimulate proliferation in hCO cultured in MM. We initially tested previously reported mitogens including growth factors, small molecules, microRNAs (miRs), and transcription factors, in commonly used neonatal rat cardiomyocyte cultures. We found that CHIR99021 (16), miR-199a (37), miR-590 (37), and overexpression of constitutively active murine YAP1(S112A) (38) were all capable of inducing mitosis in neonatal rodent cardiomyocytes marked by $pH3^+$ cardiomyocytes with disassembled sarcomeres (Fig. S8 *A* and *B*). Neuregulin (35) was unable to induce proliferation over baseline in neonatal rat cardiomyocyte cultures, although this could be caused by the presence of serum in our cultures, which induces a similar proliferative rate as neuregulin (39). We then tested whether these mitogens could induce proliferation in immature hCO (after only 6 d of culture in CTRL medium following seeding) (Fig. S8*C*). We firstly confirmed robust overexpression of miRs 48 h after transfection (Fig. S8 *D* and *E*) and very high infection efficiency (>98%) with AAV6-GFP (Fig. S8 *F* and *G*). We then screened the mitogens and found that only CHIR99021, constitutively active β-catenin (ΔN90), and constitutively active human YAP1(S127A) induced proliferation above baseline in these immature hCO (Fig. S8*H*). Interestingly, only CHIR99021 treatment resulted in a reduction of force of contraction at 48 h, indicating that it is the inhibition of GSK3 but not the activation of β-catenin or proliferation per se that results in a reduction in contractile function (Fig. S8*I*). These results confirm that Wnt/β-catenin is a highly conserved and potent regulator of cardiomyocyte proliferation in rodent and human cardiomyocytes.

We next tested whether hCOs cultured in MM were refractory to activation of proliferation using CHIR99021, which potently activated proliferation throughout immature hCO (Fig. S8 *J* and *K*). While hCOs cultured (for standard 16 d in culture) in CTRL medium mounted a robust proliferative response to CHIR99021, mature hCOs cultured in MM had a blunted proliferative response (Fig. 5 *J* and *K*). This finding suggested that mature hPSC-CMs in MM were resistant to proliferative stimuli.

The highly oxidative postnatal environment in cardiomyocytes in vivo induces a DNA damage response (DDR), which has been proposed as a central mechanism driving cardiomyocyte terminal differentiation (29). Consistent with these findings in vivo, we also found that there was increased expression of DDR proteins in hCO

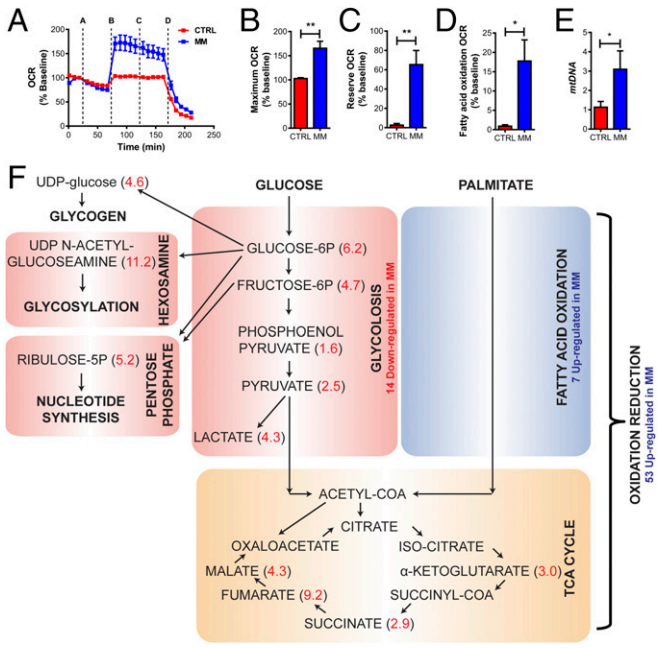

Fig. 4. Metabolism switches from glycolysis to fatty acid oxidation in hCOs cultured in MM. (*A*) Seahorse mitochondrial stress test. A, oligomycin; B, FCCP; C, etomoxir; D, antimycin A/rotenone. The Seahorse stress tests were run with n = 6 independent recordings from n = 8 pooled hCOs per recording from hCOs cultured in CTRL medium or MM for 9 d (*B*–*D*). (*B*) Maximum OCR is higher in hCOs cultured in MM. (*C*) Reserve metabolic capacity is higher in hCOs cultured in MM. (*D*) Fatty acid oxidation is higher in hCOs cultured in MM. (*E*) mtDNA is higher in hCOs cultured in MM (qPCR using *ND1* and *RNA18S5* as the nuclear DNA controls); n = 4 experiments. (*F*) Measurements of carbon metabolites (n = 2, each 12–14 pooled hCOs) confirm that the metabolism in hCOs cultured in MM switches from glycolysis to fatty acid oxidation. Values in red indicate fold higher in CTRL medium vs. MM. Metabolomics values are normalized to the DNA intensity in hCOs cultured in MM vs. CTRL medium. Data are mean ± SEM. *P < 0.05; **P < 0.01, t test (*B*–*D*) or ratio paired t test (*E*).

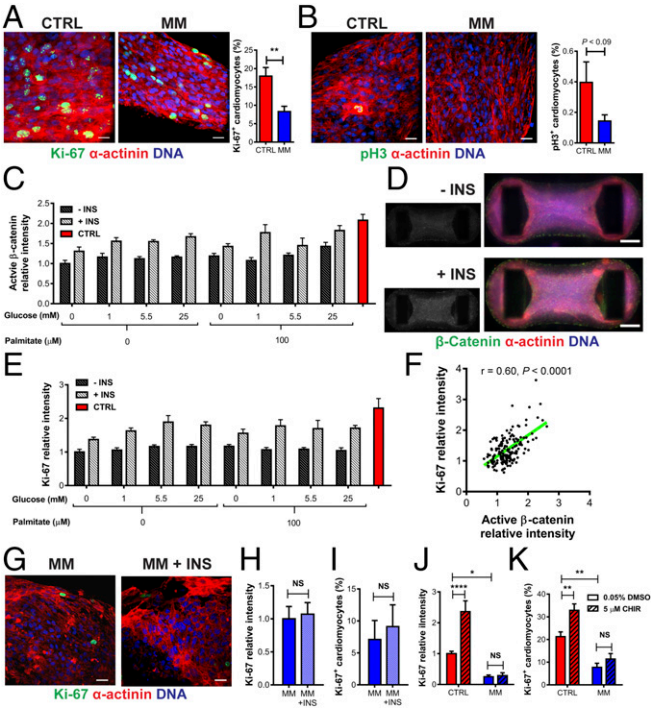

Fig. 5. hPSC-CM proliferation and WNT–β-catenin signaling are repressed in hCOs cultured in MM. (*A*) Culture of hCOs in MM reduces hPSC-CM (α-actinin) proliferation (Ki-67); n = 11–14 hCOs from three to four experiments. The 4,396 hPSC-CMs were manually counted. (Scale bars: 20 μm.) (*B*) Culture of hCOs in MM reduces hPSC-CM (α-actinin) mitosis (pH3); n = 10 from five experiments. The 7,838 hPSC-CMs were manually counted. (*C*) Activated β-catenin intensity in hCOs cultured in different metabolic conditions after 48 h reveals that lack of insulin is responsible for a decrease in activated β-catenin. Data are normalized to the 0 mM glucose, 0 μM palmitate condition; n = 6–13 from three experiments. (*D*) Representative immunostaining of activated β-catenin in hCO in MM with and without insulin. (Scale bars: 200 μm.) *Insets* are activated β-catenin alone. (*E*) Ki-67 intensity in hCOs cultured in different metabolic conditions after 48 h reveals that lack of insulin is responsible for the initial drop in cell cycle activity. Data are normalized to the 0 mM glucose, 0 μM palmitate condition; n = 6–13 from three experiments. (*F*) Cell cycle activity (Ki-67) and activated β-catenin were highly correlated in hCOs cultured under different metabolic conditions; n = 146 from three experiments. (*G*) Reintroduction of insulin for 48 h after longer term culture (9 d in MM) could not restore proliferation (Ki-67) of hPSC-CMs (α-actinin; representative immunostaining). (Scale bars: 20 μm.) (*H*) Ki-67 intensity in hCOs after reintroduction of insulin for 48 h after longer term culture (9 d in MM) could not restore proliferation; n = 10–11 hCOs from two experiments. (*I*) Quantification of proliferating (Ki-67) hPSC-CMs (α-actinin) reveals that reintroduction of insulin for 48 h after longer term culture (9 d in MM) could not restore proliferation; n = 3–4 hCOs from two experiments. The 2,441 hPSC-CMs were manually counted. (*J*) hCOs cultured in MM have a blunted proliferative response (Ki-67 intensity) to CHIR99021 (24-h treatment); n = 11–14 hCOs from three to four experiments. (*K*) Quantification of proliferating (Ki-67) hPSC-CMs (α-actinin) confirms that hCOs cultured in MM have a blunted proliferative response to CHIR99021 (24-h treatment); n = 7–8 from two experiments. The 10,609 hPSC-CMs were manually counted. Data are mean ± SEM. P values were calculated using t test (*B*, *H*, and *I*) or Pearson correlation (r) and P value (*F*). INS− is statistically different from INS+ ($P < 0.0001$) using two-way ANOVA (*C* and *E*). $^*P < 0.05$; $^{**}P < 0.01$; and $^{****}P < 0.0001$ using t test (*A*) or ANOVA with Tukey's posttest (*J* and *K*). INS, insulin.

cultured in MM (Figs. 3*G* and 6*A*). There was evidence for induction of the DDR in hCO cultured in MM, including increased expression of a marker of oxidative base modification in DNA 8-oxo-7,8-dihydroguanine (8-OxoG) (Fig. 6*B*) and increased Ser1987 phosphorylated ATM (pATM) (Fig. 6*C*). Therefore, consistent with in vivo postnatal maturation, the DDR is also associated with proliferative arrest in hCO cultured in MM.

Synergistic Activation of YAP1 and β-Catenin Results in Cell Cycle Reactivation and a Reduction in DDR. As CHIR99021 could not rescue the reduction in proliferation in MM, we next hypothesized that the β-catenin and YAP1 act in synergy to activate proliferation for a number of reasons: (*i*) both β-catenin and YAP1 activated proliferation in immature hCOs (Fig. S8*H*), (*ii*) both β-catenin and YAP1 have been shown to act cooperatively with the core cardiogenic transcription factor TBX5 to regulate the cell cycle (40), (*iii*) both β-catenin and YAP1 are required for cardiomyocyte proliferation during embryonic development (41, 42), and (*iv*) YAP1 can activate an antioxidant response in the heart (43). As YAP/TAZ mediates the transcription of the majority of its transcriptional targets through enhancers, we cross-referenced down-regulated genes in hCOs cultured in MM vs. CTRL medium (FDR < 0.05; 2,120 genes) to known YAP/TAZ targets that have been previously identified using chromatin immunoprecipitation sequencing and cross-referencing to the 3D chromatin interactome (44, 45). We found that 57 YAP/TAZ targets were significantly repressed by hCO culture in MM (Fig. 7*A*) (only 8 targets were up-regulated; a down-regulated list of gene names is in Fig. S9*A*). The YAP/TAZ targets repressed in hCOs cultured in MM included the well-characterized YAP/TAZ targets *CTGF*, *CYR61*, *ANKRD1*, and *AXL* (44). The top GO term for the repressed YAP/TAZ targets was regulation of cell cycle (10 genes, $P = 9.7 \times 10^{-4}$), thereby indicating that loss of YAP/TAZ transcriptional activity could by partially responsible for the cell cycle arrest observed in hCO cultured in MM.

We next tested whether coactivation of β-catenin and YAP1 was sufficient to drive hPSC-CM cell cycle reentry in MM-cultured hCOs and rescue the proliferative block caused by the switch in metabolism. We found that overexpression of either constitutively active YAP1 (S127A) or constitutively active β-catenin (ΔN90) alone was insufficient to facilitate cell cycle reentry in hCO cultured in MM and failed to activate *BIRC5* transcription (Fig. S9 *B–E*), which has been shown to be dependent on a β-catenin and YAP1 complex (40). However, overexpression of both β-catenin (ΔN90) and YAP1 (S127A) had a synergistic effect and together, augmented proliferation (Fig. 7*B* and Fig. S9*F*) and mitosis (Fig. 7*C*) of hPSC-CMs, as well as *BIRC5* transcription (Fig. S9*G*) in

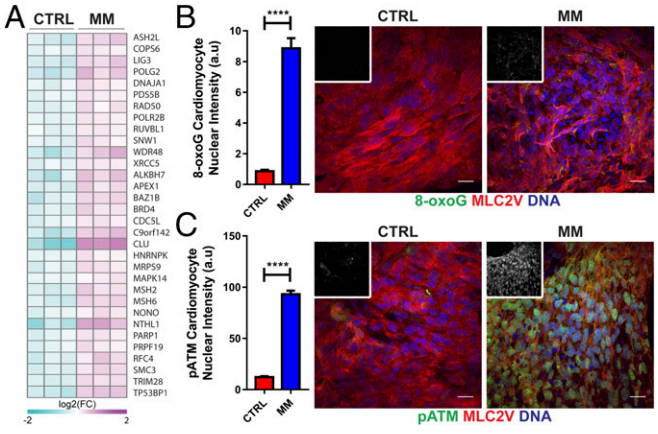

Fig. 6. hCO culture in MM induces a DDR. (*A*) Heat map showing significantly regulated proteins in CTRL medium vs. MM derived from proteomics data for the GO term cellular response to DNA damage stimulus. Data are presented as $\log_2$ expression relative to mean for all conditions; n = 3 experiments. (*B*) Nuclear intensity for the oxidative base modification in DNA, 8-OxoG, showing an increase in hPSC-CMs (MLC2v) cultured in MM; n = 120–180 hPSC-CM nuclei. *Insets* are 8-OxoG alone. (*C*) Nuclear intensity for pATM (Ser1987) showing an increase in hPSC-CM (MLC2v) cultured in MM; n = 120–240 hPSC-CM nuclei. *Insets* are pATM alone. Data are mean ± SEM. (Scale bars: 20 μm.) $^{****}P < 0.0001$ using t test (*B* and *C*).

the hCOs cultured in MM. This proliferative response did not alter the force of contraction (Fig. S9*H*).

To confirm our findings with an independent method, we coactivated both signaling pathways using a small molecule, compound 6.28 (46) (Fig. S9*I*). Compound 6.28 inhibits both GSK3A/B (IC_{50} of 13 and 16 nM, respectively) and MST1 (IC_{50} of 12 nM) (Fig. S9*J*), which are critical upstream inhibitors of β-catenin (47) and YAP1 (48), respectively. Compound 6.28 induced concentration-dependent increases in hPSC-CM proliferation (Fig. 7 *D* and *E*) and also induced mitosis (Fig. 7*F*) and activation of *BIRC5* (Fig. 7*G*) in hCOs cultured in MM. Treatment with compound 6.28 also resulted in increased DNA intensity (Fig. 7*H*) and an 11 ± 2.5% (Fig. 7*I*) increase in hCO size after 48 h without an increase in hPSC-CM size (Fig. 7*J*), indicative of bona fide proliferation. To determine the global effects of compound 6.28, we also performed proteomics and found 71 up-regulated and 20 down-regulated proteins (Fig. S9*K*). We performed GO term analysis, and consistent with our data on compound 6.28, we found that multiple aspects of cell cycle were activated, including (but not limited to) G1/S cell cycle phase transition, DNA replication, mitotic cell cycle, and cytokinesis (Fig. 7*K*). Fatty acid biosynthetic processes were also activated by compound 6.28 (Fig. 7*K*).

Taken together, our findings show that synergistic activation of β-catenin and YAP signaling induces bona fide hPSC-CM proliferation within our hCOs by rescuing the proliferative barrier imposed by culture in MM.

Discussion

hPSC-CMs have become widely used to study human cardiac biology, development, and physiology. However, they are typically immature, which limits their capacity to accurately model adult cardiac biology. While engineered heart muscle can improve hPSC-CM maturation in terms of structure and function (10, 14), the key upstream drivers of metabolic maturation and cell cycle arrest are largely unknown.

To identify central regulators of hPSC-CM maturation and cell cycle exit, we developed a miniaturized semiautomated cardiac organoid culture platform (Heart-Dyno) to facilitate screening. Through systematic and iterative screening, we were able to show that distinct physiological hallmarks of the maturation process were driven by different cues. For example, we found that maturation of many parameters, such as the structural, electrophysiological, and calcium handling as well as responses to adrenergic stimulation, were supported by the 3D engineered heart tissue environment. These parameters in our hCO were similar to those reported using other cardiac tissue engineering platforms (8–14). However, we found that switching metabolism to fatty acid oxidation was a key driver not only for shifting the expression of metabolism genes, mitochondrial biogenesis, and fatty acid oxidation but also, for increased expression of adult sarcomeric protein isoforms and cell cycle exit. Therefore, different aspects of the adult cardiomyocyte phenotype are governed by distinct cues, which need to be carefully controlled for the generation of mature hPSC-CMs.

During the first week of the postnatal period in vivo, a metabolic switch to fatty acid oxidation and cell cycle exit occurs in the heart in concert with a change in serum composition from glycolytic substrates to fatty acids (4). In this study, we found that mimicking these changes in metabolic substrate provision is a major driver of not only the metabolic maturation but also, the transcriptional and cell cycle maturation in human cardiomyocytes. Specifically, we found that a switch from commonly used high-insulin, carbohydrate-based medium to a low-carbohydrate, low-insulin, palmitate-based medium enhanced the maturation of hCOs. These maturation conditions are in contrast to the typical cell growth environments, which generally include glucose, insulin, and serum and are designed to increase cellular proliferation. Altering the metabolic environment was critical to promote maturation in hCO and may also represent a viable approach for promoting differentiation and functional maturation of other cell types.

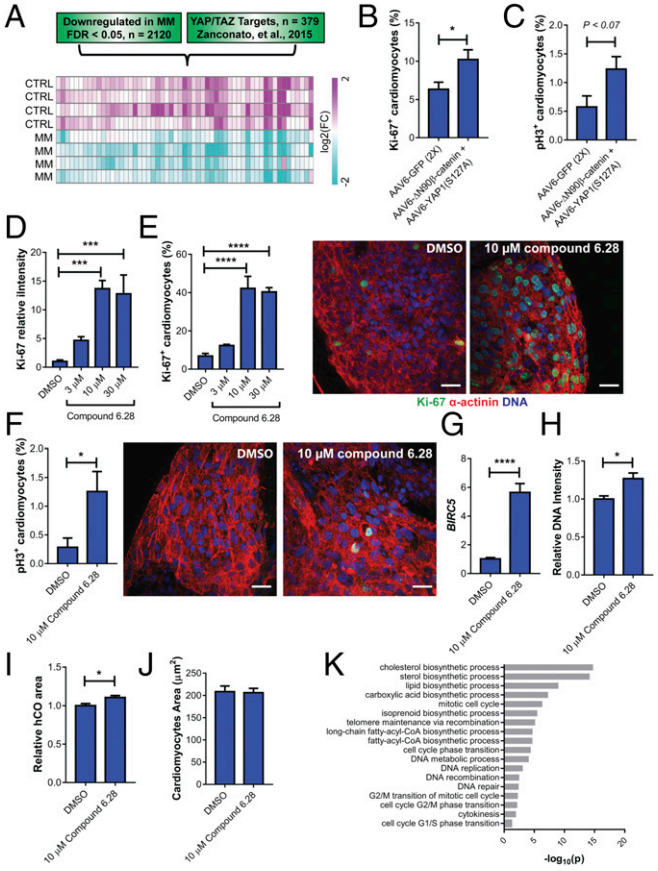

Fig. 7. β-Catenin and YAP1 coactivation restores proliferation in MM. (*A*) YAP/TAZ target genes are repressed in hCOs cultured in MM. Heat map data from significantly regulated YAP/TAZ targets in RNA-seq data; $n = 4$ experiments. (*B*) Delivery of constitutively active β-catenin and YAP1 cooperate to activate proliferation (Ki-67) of hPSC-CMs (α-actinin) in hCOs cultured in MM; $n = 9$ from three experiments. The 10,434 hPSC-CMs were manually counted. (*C*) Delivery of constitutively active β-catenin and YAP1 cooperate to induce mitosis (pH3) in hPSC-CMs (α-actinin) in hCOs cultured in MM; $n = 3$–4. The 3,770 hPSC-CMs were manually counted. (*D*) Compound 6.28 induces dose-dependent increases in proliferation (Ki-67 intensity) in hCOs cultured in MM for 2 d; $n = 6$–9 from two experiments. (*E*) Compound 6.28 induces dose-dependent increases in proliferation (Ki-67) of hPSC-CMs (α-actinin) in hCOs cultured in MM. Representative images of proliferating (Ki-67) hPSC-CMs (α-actinin) treated with DMSO or compound 6.28 for 2 d; $n = 6$–9 from two experiments. The 10,742 hPSC-CMs were manually counted. (*F*) Compound 6.28 induces mitosis (pH3) of hPSC-CMs (α-actinin) in hCOs cultured in MM. Representative images of mitotic (pH3) of hPSC-CMs (α-actinin) treated with DMSO or compound 6.28 for 2 d; $n = 7$ from two experiments. The 4,782 hPSC-CMs were manually counted. (*G*) Compound 6.28 induces expression of *BIRC5* in hCOs cultured in MM; $n = 5$–6. (*H*) DNA intensity increases in hCO treated with compound 6.28 for 2 d; $n = 7$–9 hCOs from two experiments. (*I*) hCO area (using α-actinin area) increases after treatment with compound 6.28 for 2 d; $n = 7$–9 hCOs from two experiments. (*J*) Average hPSC-CM area per image does not change after treatment with compound 6.28 for 2 d; $n = 13$–15 hCOs from two experiments. (*K*) GO term analysis of proteomics reveals that multiple fatty acid biosynthesis and cell cycle processes are increased in hCOs treated with compound 6.28 for 2 d. Data are mean ± SEM. $^*P < 0.05$; $^{***}P < 0.001$; and $^{****}P < 0.0001$, using ANOVA with Dunnet's posttest (*D* and *E*) or *t* test (*B*, *C*, and *F*–*I*).

Recent studies have suggested that oxygen tension is linked to cardiomyocyte proliferation (28, 29, 49) and revealed that a high oxygen environment is a key trigger for postnatal cardiomyocyte cell cycle exit (29). However, the in vitro culture of hPSC-CMs at atmospheric oxygen (~21% O_2) is not sufficient to drive cell

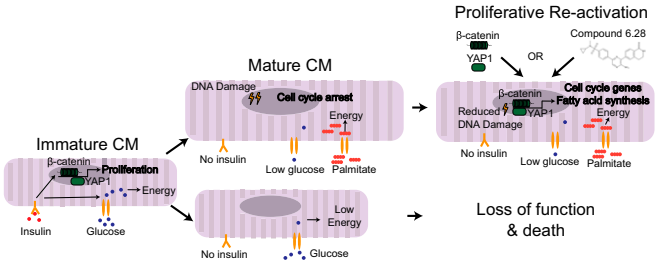

Fig. 8. Metabolism regulates cardiac maturation. Insulin can only be removed in long-term culture with maintenance of contractile function if fatty acids replace glucose substrates. Initially, the removal of insulin is responsible for a decrease in proliferation. However, in the longer term, cell cycle arrest cannot be rescued by addition of insulin, because there are alterations in metabolism, which repress β-catenin and YAP1 signaling and induce a DDR, thus resulting in cell cycle exit. CM, cardiomyocyte.

cycle exit (16, 50). Our study shows that a switch to fatty acid oxidation via alteration of metabolic substrate utilization, in a high oxygen environment, is a driver of hPSC-CM cell cycle arrest. This suggests that the high oxygen environment works in concert with changes in metabolic substrate availability after birth to govern cardiomyocyte cell cycle arrest. This is also supported in vivo by a recent study showing a link between reduced oxygen concentrations and reactivation of cardiomyocyte proliferation and cardiac regeneration in the adult heart, which was associated with a metabolic switch to glycolysis (28). Together, these studies establish a causal link between postnatal metabolic adaptations, oxygen tension, and cardiomyocyte proliferation.

Our findings show that switching hPSC-CM metabolism to fatty acid oxidation induces long-lasting changes in β-catenin and YAP1 signaling as well as the DDR, which results in hPSC-CM cell cycle withdrawal. Importantly, simultaneous activation of β-catenin and YAP1 was required to overcome the metabolism-induced proliferative barrier in mature hCO. Cooperativity between β-catenin and YAP signaling has also been reported in the embryonic heart, where they interact to control cardiomyocyte proliferation during heart development (41). Moreover, Hippo/Yap signaling has emerged as a central regulator of cardiac regenerative capacity in the neonatal period (38, 51). Our study suggests that postnatal alterations in cardiomyocyte metabolism could operate as a key switch leading to cardiomyocyte cell cycle shut down via repression of β-catenin and YAP signaling after birth. Similarly, alterations in metabolism are known to influence β-catenin and YAP activity in other cell types (52, 53). Therefore, these findings support a model, whereby β-catenin, YAP1, metabolism, and the DDR are intimately linked and cooperate to regulate the cardiac cell cycle and maturation (Fig. 8).

Although the mechanisms by which β-catenin and YAP1 interact to induce cell cycle reentry in metabolically mature cardiomyocytes require additional elucidation, we found that treatment with compound 6.28 activates fatty acid synthesis pathways and reduces the DDR in mature hCO. These findings are of particular interest, because fatty acid biosynthesis plays a key role in tumorigenesis (54). Key regulators of fatty acid biosynthesis that are up-regulated by compound 6.28 include fatty acid synthase and ATP citrate lyase, which are currently being pursued as targets for cancer therapeutics (54). While fatty acid synthesis can regulate many biological processes and signaling pathways, it can also protect cells from reactive oxygen species by altering the overall saturation levels of lipids in the cell membrane (54). Additionally, YAP1 has been implicated in cardiac regeneration by promoting an antioxidant response (43). In support of this notion, treatment with compound 6.28 also reduced pATM levels (Fig. S10 *A* and *B*) and decreased the expression levels of *RAD50* and *PARP1* (Fig. S10*C*), suggesting that β-catenin and YAP1 coactivation may be an approach to overcome the proliferative barrier imposed by the postnatal DDR in cardiomyocytes (29).

The production of human organoids has rapidly advanced over the past few years. Coupled with higher throughput screening platforms, such as the Heart-Dyno, organoid experiments have the potential to rapidly expand our knowledge of human biology and potentially unlock therapeutic strategies for many diseases.

Methods

Heart-Dyno Fabrication. Heart-Dyno culture inserts were fabricated using standard SU-8 photolithography and PDMS molding practices (16).

Neonatal Rat Ventricular Cardiomyocytes. Cardiomyocytes were derived from P1 Sprague–Dawley neonatal rats; 1- to 2-d-old neonatal rats (Sprague–Dawley) were used for cardiomyocyte isolation and handled in accordance with the Australian code of practice for care and use of animals for scientific purposes under ethics approval from the University of Queensland Ethics Committee.

Human Samples. Ethical approval for the use of hESCs was obtained from The University of Queensland's Medical Research Ethics Committee (2014000801), and the human adult heart sample for proteomics was obtained under ethical approval from The University of Sydney (2012/2814). Ethical approval was carried out in accordance with the National Health and Medical Research Council of Australia regulations under informed consent. The adult human heart sample was obtained from Clontech.

Cardiac Differentiation and hCO Fabrication. Cardiac cells were produced using recently developed protocols (13, 55, 56). For each hCO, 5×10^4 cardiac cells were mixed with collagen I to make a 3.5-μl final solution containing 2.6 mg/ml collagen I and 9% Matrigel. The bovine acid-solubilized collagen I (Devro) was first salt-balanced and pH-neutralized using 10X DMEM and 0.1 M NaOH, respectively, prior to mixing with Matrigel and cells. The mixture was prepared on ice and pipetted into the Heart-Dyno; more details are in *SI Methods*.

hCO Screening and Characterization. Methods associated with hCO screening and characterization, including force analysis, staining and imaging, hPSC-CM dissociation, electrophysiology, calcium imaging, RNA extraction, qPCR, RNA-seq, proteomics, TEM, bioinformatics analysis, metabolite analysis, and metabolic profiling, can be found in *SI Methods*. Details of antibodies (Table S1) and primers (Table S2) can be found in *SI Methods*.

ACKNOWLEDGMENTS. We thank Shaun Walters for his assistance in setting up the customized Leica DMI8 microscope for our applications and Dr. Sean Lal (Sydney Heart Bank) for providing the human heart biopsy for proteomic analysis. We thank the Developmental Studies Hybridoma Bank for providing the β-catenin (PY489) and titin antibodies. We used the Australian National Fabrication Facility Queensland Node for the fabrication of the Heart-Dyno molds. We also thank QFAB bioinformatics for access to MetaCore as well as the GVL project and the Research Computing Centre for access to the Galaxy-qld server (https://galaxy-qld.genome.edu.au/galaxy). We acknowledge the use of the Australian Microscopy & Microanalysis Research Facility at the Center for Microscopy and Microanalysis at The University of Queensland. R.G.P. was supported by National Health and Medical Research Council of Australia Grants APP1037320, APP1058565, and APP569542 and the Australian Research Council Centre of Excellence in Convergent Bio-Nano Science and Technology. D.A.E. and E.R.P. are supported by the Victorian Government's Operational Infrastructure Support Program. E.R.P. and J.E.H. are supported by fellowships and project grants from the National Health and Medical Research Council, the National Heart Foundation, Stem Cells Australia, and The University of Queensland.

1. Porrello ER, Olson EN (2014) A neonatal blueprint for cardiac regeneration. *Stem Cell Res (Amst)* 13:556–570.
2. Porrello ER, et al. (2013) Regulation of neonatal and adult mammalian heart regeneration by the miR-15 family. *Proc Natl Acad Sci USA* 110:187–192.
3. Porrello ER, et al. (2011) Transient regenerative potential of the neonatal mouse heart. *Science* 331:1078–1080.
4. Girard J, Ferré P, Pégorier JP, Duée PH (1992) Adaptations of glucose and fatty acid metabolism during perinatal period and suckling-weaning transition. *Physiol Rev* 72:507–562.

5. Sim CB, et al. (2015) Dynamic changes in the cardiac methylome during postnatal development. *FASEB J* 29:1329–1343.
6. Shekhawat PS, Matern D, Strauss AW (2005) Fetal fatty acid oxidation disorders, their effect on maternal health and neonatal outcome: Impact of expanded newborn screening on their diagnosis and management. *Pediatr Res* 57: 78R–86R.
7. Tiburcy M, Zimmermann WH (2014) Modeling myocardial growth and hypertrophy in engineered heart muscle. *Trends Cardiovasc Med* 24:7–13.
8. Boudou T, et al. (2012) A microfabricated platform to measure and manipulate the mechanics of engineered cardiac microtissues. *Tissue Eng Part A* 18:910–919.
9. Tulloch NL, et al. (2011) Growth of engineered human myocardium with mechanical loading and vascular coculture. *Circ Res* 109:47–59.
10. Zhang D, et al. (2013) Tissue-engineered cardiac patch for advanced functional maturation of human ESC-derived cardiomyocytes. *Biomaterials* 34:5813–5820.
11. Schaaf S, et al. (2011) Human engineered heart tissue as a versatile tool in basic research and preclinical toxicology. *PLoS One* 6:e26397.
12. Nunes SS, et al. (2013) Biowire: A platform for maturation of human pluripotent stem cell-derived cardiomyocytes. *Nat Methods* 10:781–787.
13. Voges HK, et al. (2017) Development of a human cardiac organoid injury model reveals innate regenerative potential. *Development* 144:1118–1127.
14. Tiburcy M, et al. (2017) Defined engineered human myocardium with advanced maturation for applications in heart failure modeling and repair. *Circulation* 135: 1832–1847.
15. Zimmermann WH, et al. (2006) Engineered heart tissue grafts improve systolic and diastolic function in infarcted rat hearts. *Nat Med* 12:452–458.
16. Titmarsh DM, et al. (2016) Induction of human iPSC-derived cardiomyocyte proliferation revealed by combinatorial screening in high density microbioreactor arrays. *Sci Rep* 6:24637.
17. Bougnères PF, Karl IE, Hillman LS, Bier DM (1982) Lipid transport in the human newborn. Palmitate and glycerol turnover and the contribution of glycerol to neonatal hepatic glucose output. *J Clin Invest* 70:262–270.
18. Tiburcy M, et al. (2011) Terminal differentiation, advanced organotypic maturation, and modeling of hypertrophic growth in engineered heart tissue. *Circ Res* 109: 1105–1114.
19. Desbois-Mouthon C, et al. (2001) Insulin and IGF-1 stimulate the beta-catenin pathway through two signalling cascades involving GSK-3beta inhibition and Ras activation. *Oncogene* 20:252–259.
20. Racca AW, et al. (2016) Contractile properties of developing human fetal cardiac muscle. *J Physiol* 594:437–452.
21. Moreo A, et al. (2009) Influence of myocardial fibrosis on left ventricular diastolic function: Noninvasive assessment by cardiac magnetic resonance and echo. *Circ Cardiovasc Imaging* 2:437–443.
22. Zimmermann WH, et al. (2002) Tissue engineering of a differentiated cardiac muscle construct. *Circ Res* 90:223–230.
23. Eder A, Vollert I, Hansen A, Eschenhagen T (2016) Human engineered heart tissue as a model system for drug testing. *Adv Drug Deliv Rev* 96:214–224.
24. Yang X, Pabon L, Murry CE (2014) Engineering adolescence: Maturation of human pluripotent stem cell-derived cardiomyocytes. *Circ Res* 114:511–523.
25. Kuppusamy KT, et al. (2015) Let-7 family of microRNA is required for maturation and adult-like metabolism in stem cell-derived cardiomyocytes. *Proc Natl Acad Sci USA* 112:E2785–E2794.
26. Pinto AR, et al. (2016) Revisiting cardiac cellular composition. *Circ Res* 118:400–409.
27. DeLaughter DM, et al. (2016) Single-cell resolution of temporal gene expression during heart development. *Dev Cell* 39:480–490.
28. Nakada Y, et al. (2017) Hypoxia induces heart regeneration in adult mice. *Nature* 541: 222–227.
29. Puente BN, et al. (2014) The oxygen-rich postnatal environment induces cardiomyocyte cell-cycle arrest through DNA damage response. *Cell* 157:565–579.
30. Dubois NC, et al. (2011) SIRPA is a specific cell-surface marker for isolating cardiomyocytes derived from human pluripotent stem cells. *Nat Biotechnol* 29:1011–1018.
31. Nelson DO, Jin DX, Downs KM, Kamp TJ, Lyons GE (2014) Irx4 identifies a chamber-specific cell population that contributes to ventricular myocardium development. *Dev Dyn* 243:381–392.
32. Bruneau BG, et al. (2001) Cardiomyopathy in Irx4-deficient mice is preceded by abnormal ventricular gene expression. *Mol Cell Biol* 21:1730–1736.
33. Jiang J, et al. (2015) Cardiac myosin binding protein C regulates postnatal myocyte cytokinesis. *Proc Natl Acad Sci USA* 112:9046–9051.
34. Readnower RD, Brainard RE, Hill BG, Jones SP (2012) Standardized bioenergetic profiling of adult mouse cardiomyocytes. *Physiol Genomics* 44:1208–1213.
35. Polizzotti BD, et al. (2015) Neuregulin stimulation of cardiomyocyte regeneration in mice and human myocardium reveals a therapeutic window. *Sci Transl Med* 7: 281ra45.
36. Sturzu AC, et al. (2015) Fetal mammalian heart generates a robust compensatory response to cell loss. *Circulation* 132:109–121.
37. Eulalio A, et al. (2012) Functional screening identifies miRNAs inducing cardiac regeneration. *Nature* 492:376–381.
38. Xin M, et al. (2013) Hippo pathway effector Yap promotes cardiac regeneration. *Proc Natl Acad Sci USA* 110:13839–13844.
39. Zhao YY, et al. (1998) Neuregulins promote survival and growth of cardiac myocytes. Persistence of ErbB2 and ErbB4 expression in neonatal and adult ventricular myocytes. *J Biol Chem* 273:10261–10269.
40. Rosenbluh J, et al. (2012) β-Catenin-driven cancers require a YAP1 transcriptional complex for survival and tumorigenesis. *Cell* 151:1457–1473.
41. Heallen T, et al. (2011) Hippo pathway inhibits Wnt signaling to restrain cardiomyocyte proliferation and heart size. *Science* 332:458–461.
42. Xin M, et al. (2011) Regulation of insulin-like growth factor signaling by Yap governs cardiomyocyte proliferation and embryonic heart size. *Sci Signal* 4:ra70.
43. Tao G, et al. (2016) Pitx2 promotes heart repair by activating the antioxidant response after cardiac injury. *Nature* 534:119–123.
44. Zanconato F, et al. (2015) Genome-wide association between YAP/TAZ/TEAD and AP-1 at enhancers drives oncogenic growth. *Nat Cell Biol* 17:1218–1227.
45. Jin F, et al. (2013) A high-resolution map of the three-dimensional chromatin interactome in human cells. *Nature* 503:290–294.
46. Augeri DJ, et al. (2012) Patent WO/2012/121992, Germany.
47. Clevers H (2006) Wnt/beta-catenin signaling in development and disease. *Cell* 127: 469–480.
48. Xu CM, et al. (2013) Mst1 overexpression inhibited the growth of human non-small cell lung cancer in vitro and in vivo. *Cancer Gene Ther* 20:453–460.
49. Kimura W, et al. (2015) Hypoxia fate mapping identifies cycling cardiomyocytes in the adult heart. *Nature* 523:226–230.
50. Burridge PW, et al. (2014) Chemically defined generation of human cardiomyocytes. *Nat Methods* 11:855–860.
51. Morikawa Y, et al. (2015) Actin cytoskeletal remodeling with protrusion formation is essential for heart regeneration in Hippo-deficient mice. *Sci Signal* 8:ra41.
52. Wang W, et al. (2015) AMPK modulates Hippo pathway activity to regulate energy homeostasis. *Nat Cell Biol* 17:490–499.
53. Chocarro-Calvo A, García-Martínez JM, Ardila-González S, De la Vieja A, García-Jiménez C (2013) Glucose-induced β-catenin acetylation enhances Wnt signaling in cancer. *Mol Cell* 49:474–486.
54. Röhrig F, Schulze A (2016) The multifaceted roles of fatty acid synthesis in cancer. *Nat Rev Cancer* 16:732–749.
55. Hudson J, Titmarsh D, Hidalgo A, Wolvetang E, Cooper-White J (2012) Primitive cardiac cells from human embryonic stem cells. *Stem Cells Dev* 21:1513–1523.
56. Zimmermann W-H, Hudson JE, Tiburcy M (2015) Patent WO 2015/040142 Al, Germany.
57. Wang H, et al. (2013) Necking and failure of constrained 3D microtissues induced by cellular tension. *Proc Natl Acad Sci USA* 110:20923–20928.
58. Thomas WG, et al. (2002) Adenoviral-directed expression of the type 1A angiotensin receptor promotes cardiomyocyte hypertrophy via transactivation of the epidermal growth factor receptor. *Circ Res* 90:135–142.
59. Bolger AM, Lohse M, Usadel B (2014) Trimmomatic: A flexible trimmer for Illumina sequence data. *Bioinformatics* 30:2114–2120.
60. Dobin A, et al. (2013) STAR: Ultrafast universal RNA-seq aligner. *Bioinformatics* 29: 15–21.
61. Cox J, et al. (2011) Andromeda: A peptide search engine integrated into the MaxQuant environment. *J Proteome Res* 10:1794–1805.
62. Tyanova S, Temu T, Cox J (2016) The MaxQuant computational platform for mass spectrometry-based shotgun proteomics. *Nat Protoc* 11:2301–2319.
63. Cox J, et al. (2014) Accurate proteome-wide label-free quantification by delayed normalization and maximal peptide ratio extraction, termed MaxLFQ. *Mol Cell Proteomics* 13:2513–2526.
64. Cox J, Mann M (2012) 1D and 2D annotation enrichment: A statistical method integrating quantitative proteomics with complementary high-throughput data. *BMC Bioinformatics* 13 Suppl 16:S12.
65. Robinson MD, McCarthy DJ, Smyth GK (2010) edgeR: A bioconductor package for differential expression analysis of digital gene expression data. *Bioinformatics* 26:139–140.
66. Huang da W, Sherman BT, Lempicki RA (2009) Systematic and integrative analysis of large gene lists using DAVID bioinformatics resources. *Nat Protoc* 4:44–57.
67. Takasato M, et al. (2015) Kidney organoids from human iPS cells contain multiple lineages and model human nephrogenesis. *Nature* 526:564–568.
68. Dietmair S, Timmins NE, Gray PP, Nielsen LK, Kromer JO (2010) Towards quantitative metabolomics of mammalian cells: Development of a metabolite extraction protocol. *Anal Biochem* 404:155–164.
69. Medina-Torres CE, van Eps AW, Nielsen LK, Hodson MP (2015) A liquid chromatography-tandem mass spectrometry-based investigation of the lamellar interstitial metabolome in healthy horses and during experimental laminitis induction. *Vet J* 206:161–169.
70. Nicholls DG, et al. (2010) Bioenergetic profile experiment using C2C12 myoblast cells. *J Vis Exp* (46).